

A hybrid finite element/finite difference method for reconstruction of dielectric properties of conductive objects

E. Lindström* L. Beilina†

October 1, 2024

Abstract

The aim of this article is to present a hybrid finite element/finite difference method which is used for reconstructions of electromagnetic properties within a realistic breast phantom. This is done by studying the mentioned properties' (electric permittivity and conductivity in this case) representing coefficients in a constellation of Maxwell's equations. This information is valuable since these coefficient can reveal types of tissues within the breast, and in applications could be used to detect shapes and locations of tumours.

Because of the ill-posed nature of this coefficient inverse problem, we approach it as an optimization problem by introducing the corresponding Tikhonov functional and in turn Lagrangian. These are then minimized by utilizing an interplay between finite element and finite difference methods for solutions of direct and adjoint problems, and thereafter by applying a conjugate gradient method to an adaptively refined mesh.

Keywords: *Maxwell's equations, finite element method, finite difference method, adaptive methods, coefficient inverse problems, microwave imaging*

MSC codes: *65J22; 65K10; 65M32; 65M55; 65M60; 65M70*

1 Introduction

In this work is presented a method of determination of the spatially distributed complex dielectric permittivity function in conductive media using scattered time-dependent data of the electric field at the boundary of investigated domain. Such problems are called Coefficient Inverse Problems (CIPs) and conventionally are solved via minimization of a least-squares residual functional using different methods – see, for example, [1, 2, 10, 11, 12, 14, 15, 13, 23, 25]. The algorithm of this paper is of a great

*Eric Lindström, Email: erilinds@chalmers.se

†Larisa Beilina, Email: larisa@chalmers.se

Department of Mathematical Sciences, Chalmers University of Technology and University of Gothenburg, SE-412 96 Gothenburg Sweden, published in 2024 International Conference on Electromagnetics in Advanced Applications (ICEAA)

need due to many real world applications where the physical model can be described by the time-dependent Maxwell's system for the electric field - see some of them in [2, 23, 25].

In works [3, 6, 7, 20, 21] were developed methods of reconstruction of dielectric permittivity function where the scalar wave equation was taken as an approximate mathematical model to the Maxwell's equations. Particularly, the two-stage adaptive optimization method was developed in [3] for improvement of reconstruction of the dielectric permittivity function. The two-stage numerical procedure of [3] was verified on experimental data collected by the microwave scattering facility in several works – see, for example, [6, 7, 20, 21]. In [19], see also references therein, authors show reconstruction of complex dielectric permittivity function using convexification method and frequency-dependent data. Potential applications of above cited works are in the detection and characterization of improvised explosive devices (IEDs).

One of the most important applications of algorithm of this paper is microwave medical imaging and imaging of improvised explosive devices (IEDs) where is needed qualitative and quantitative determination of both, the dielectric permittivity and electric conductivity functions, from boundary measurements. Microwave medical imaging, when only boundary measurements of backscattered electric waves at frequencies around 1 GHz are used, is non-invasive imaging. Thus, it is very attractive complement to the existing imaging technologies like X-ray or ultrasound imaging.

Potential application of algorithm developed in this work is in breast cancer detection. Different malign-to-normal tissues contrasts are reported in [24] revealing that malign tumors have a higher water/liquid content, and thus, higher relative permittivity and conductivity values, than normal tissues. The challenge of any computational reconstruction algorithm is to accurately estimate the relative permittivity of the internal structures using the information from the backscattered electromagnetic waves collected at several detectors. In numerical simulations presented in the paper we will focus on microwave medical imaging of breast phantom provided by online repository [28] using time-dependent backscattered data of the electric field collected at the transmitted boundary of the computational domain.

In this work we briefly present finite element/finite difference (FE/FD) domain decomposition method (DDM) for numerical solution of Maxwell's equations in conductive media. We refer to [8, 9] for the full details of this method. The reconstruction algorithm of this work is new and uses DDM method for qualitative and quantitative reconstruction of dielectric properties of breast phantom taken from database [28] using simulated data in 3D.

2 Forward problem

Throughout this paper we will restrict our problem to a bounded, convex domain $\Omega \subset \mathbb{R}^d, d = 2, 3$, with a smooth boundary Γ . Since we will consider a time-dependent problem we will also make use of the notations $\Omega_T := \Omega \times (0, T)$ and $\Gamma_T := \Gamma \times (0, T)$ for corresponding space-time domains, with some end time $T > 0$. We will also restrict ourselves to isotropic and linear materials, which lets us study the following constella-

tion of Maxwell's equations:

$$\mu \partial_t H = -\nabla \times E \quad \text{in } \Omega_T, \quad (1)$$

$$\varepsilon \partial_t E = \nabla \times H - \sigma E, \quad \text{in } \Omega_T, \quad (2)$$

$$\nabla \cdot \varepsilon E = 0 \quad \text{in } \Omega_T, \quad (3)$$

$$E(x, 0) = f_0(x), \quad \partial_t E(x, 0) = f_1(x) \quad \text{in } \Omega, \quad (4)$$

$$\partial_n E = -\partial_t E \quad \text{on } \Gamma_T. \quad (5)$$

Here $E(x, t)$ and $H(x, t)$ are time-dependent vector fields mapping to \mathbb{R}^d which represents the electric and the magnetic field, respectively. We also made use of Ohm's law to replace the conventionally denoted vector field J , the dielectric current density, with σE in (2). Besides these fields we also have three coefficients ε , σ and μ which describe the electric permittivity, the conductivity and the magnetic permeability of the medium, correspondingly. Finally we have f_0 and f_1 which are arbitrary initial conditions.

To write the system (1)–(5) in terms of E , we first take the time-derivative of (2) and insert (1) into it. This gives us the equation

$$\varepsilon \partial_{tt} E + \sigma \partial_t E + \nabla \times \left(\frac{1}{\mu} \nabla \times E \right) = 0 \quad \text{in } \Omega_T. \quad (6)$$

The permittivity $\varepsilon := \varepsilon_r \varepsilon_0$ and permeability $\mu = \mu_r \mu_0$ consist of one component that is relative to the medium (denoted with the subscript r) and one component that is constant and defined in vacuum (denote with the subscript 0). In this article we will make an empirically informed approximation and let $\mu_r = 1$. With this and the well-known connection with the speed of light $c = (\varepsilon_0 \mu_0)^{-1/2}$ we can now rewrite (6) as

$$\frac{\varepsilon_r}{c^2} \partial_{tt} E + \mu_0 \sigma \partial_t E + \nabla \times \nabla \times E = 0 \quad \text{in } \Omega_T. \quad (7)$$

Since the constants before the two first terms in (7) are so small we will make a change of variables with $t \rightarrow ct$. For the sake of brevity we also drop the subscript on ε_r , as well as denote $\sigma := c \mu_0 \sigma$. This grants us the more concise Cauchy problem

$$\varepsilon \partial_{tt} E + \sigma \partial_t E + \nabla \times \nabla \times E = 0 \quad \text{in } \Omega_T, \quad (8)$$

$$\nabla \cdot \varepsilon E = 0 \quad \text{in } \Omega_T, \quad (9)$$

We observe that the boundary condition in (5) is the first order absorbing boundary condition for the wave equation, and it is justified in the next section why we are using it here. Yet we are not quite done in terms of our forward problem. In our implementations we wish to use $P1$ -elements, and it is well-known that if we apply this to (8)–(9) we risk to get spurious solutions – see, for example, [16, 17, 18]. To remedy this, we introduce (9) in (8) as a stabilizing, Coloumb gauge-type term [17, 18]. Simultaneously, we will expand the double curl term with the identity $\nabla \times \nabla \times E = \nabla \nabla \cdot E - \Delta E$.

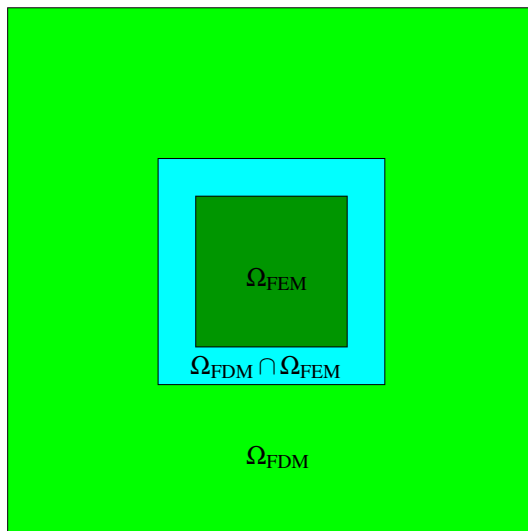


Figure 1: *Picture of domain decomposition* $\Omega := \Omega_{\text{FDM}} \cup \Omega_{\text{FEM}}$.

This gives us the final system

$$\varepsilon \partial_{tt} E + \sigma \partial_t E - \Delta E - \nabla \nabla \cdot (\varepsilon - 1) E = 0 \quad \text{in } \Omega_T, \quad (10)$$

$$E(x, 0) = f_0(x), \quad \partial_t E(x, 0) = f_1(x) \quad \text{in } \Omega, \quad (11)$$

$$\partial_n E = -\partial_t E \quad \text{on } \Gamma_T. \quad (12)$$

The system above is stable and shown in [4, 9] that it approximates (1)–(5).

Forward problem: Find E that solves problem (10)–(12) for given functions ε , σ , f_0 and f_1 .

3 Inverse problem

Before we state the inverse problem we will discuss our domain decomposition (see Fig. 1). The domain is divided such that $\Omega =: \Omega_{\text{FDM}} \cup \Omega_{\text{FEM}}$, $\overline{\Omega_{\text{FEM}}} \subset \Omega$ where $\partial \Omega_{\text{FEM}} \subset \Omega_{\text{FDM}}$. The notation of these sets will be clarified when we discuss the implementations. Within this domain we also have some assumptions on ε and σ :

$$\begin{aligned} \varepsilon(x) = 1, \quad \sigma(x) = 0 & \quad \text{in } \Omega_{\text{FDM}}, \\ 1 \leq \varepsilon(x) \leq \bar{\varepsilon}, \quad 0 \leq \sigma(x) \leq \bar{\sigma} & \quad \text{in } \Omega \setminus \Omega_{\text{FDM}}, \end{aligned} \quad (13)$$

where $\bar{\varepsilon}$ and $\bar{\sigma}$ are constant upper bounds. Note that these assumptions are particularly useful for the forward problem, since we essentially have a wave equation within Ω_{FDM} . This also motivates using the absorbing boundary condition (12) instead of, for

example, perfectly conducting boundary conditions. This setup is sufficient to state our inverse problem.

Inverse problem: Assume that ε and σ follow assumptions (13) with known $\bar{\varepsilon}$ and $\bar{\sigma}$. Determine ε and σ in $\Omega \setminus \Omega_{\text{FDM}}$ such that

$$E = E_{\text{obs}}, \quad \text{on } \Gamma_T, \quad (14)$$

where E is the corresponding forward solution and E_{obs} are some measurements made at the boundary.

4 Tikhonov functional and Lagrangian

Since our inverse problem is ill-posed we will approach it as an optimization problem. However, some notation will be introduced ahead to make the following equations more brief. We will use the standard L^2 inner products and accompanying norms, notated as

$$(f, g)_A := \int_A fg \, dA, \quad (15)$$

$$\|f\|_A := (f, f)_A^{1/2}. \quad (16)$$

To reduce notations, since $(\cdot, \cdot)_{\Omega_T}$ will come up particularly frequently we will omit this subscript and let $(\cdot, \cdot) := (\cdot, \cdot)_{\Omega_T}$ and $\|\cdot\| := \|\cdot\|_{\Omega_T}$. We will also make use of the weighted norm for functions $w \geq 0$

$$\|f\|_{w,A} := (wf, f)_A^{1/2}. \quad (17)$$

Our regularized Tikhonov functional is now defined as

$$\begin{aligned} J(E, \varepsilon, \sigma) &:= \frac{1}{2} \|E - E_{\text{obs}}\|_{z, \Gamma_T}^2 \\ &+ \frac{\gamma_\varepsilon}{2} \|\varepsilon - \varepsilon^0\|_\Omega^2 + \frac{\gamma_\sigma}{2} \|\sigma - \sigma^0\|_\Omega^2, \end{aligned} \quad (18)$$

where z is a function which ensures compatibility between E and E_{obs} , γ_ε and γ_σ are regularization parameters and ε^0 and σ^0 are initial guesses of ε and σ , respectively.

To minimize J directly is a difficult task however. In this article we aim to use a conjugate gradient method, and the Frechét derivative of our Tikhonov functional is complicated to express since E as the forward solution, and is dependent on both ε and σ . What we do instead is that we introduce our corresponding Lagrangian in a weak form:

$$\begin{aligned} L(E, \lambda, \varepsilon, \sigma) &:= J(E, \varepsilon, \sigma) - (\lambda(x, 0), f_1)_\varepsilon - (\partial_t \lambda, \partial_t E)_\varepsilon + (\lambda, \partial_t E)_\sigma + (\lambda, \partial_t E)_{\Gamma_T} \\ &+ (\nabla \lambda, \nabla E) + (\nabla \cdot \lambda, \nabla \cdot (1 - \varepsilon)E), \end{aligned} \quad (19)$$

where $\lambda(x, t)$ is our Lagrange multiplier and the added terms comes from the variational formula of our forward problem. As for the domain of L , we consider elements $u :=$

$(E, \lambda, \varepsilon, \sigma) \in U := [H^1(\Omega_T)]^d \times H_\lambda^1 \times C^2(\Omega) \times C^2(\Omega)$ where

$$H_\lambda^1 := \{w \in [H^1(\Omega_T)]^d : w(T) = \partial_t w(T) = 0\}. \quad (20)$$

To minimize L , we will make use of its four Frechét derivatives. If we let $\tilde{u} := (\tilde{E}, \tilde{\lambda}, \tilde{\varepsilon}, \tilde{\sigma}) \in U$ be an arbitrary direction, then

$$\begin{aligned} \frac{\partial L}{\partial E}(u)(\tilde{E}) &= (E - E_{\text{obs}}, \tilde{E})_{z, \Gamma_T} - (\partial_t \lambda(x, 0), \tilde{E}(x, 0))_\varepsilon - (\partial_t \lambda, \partial_t \tilde{E})_\varepsilon - (\partial_t \lambda, \tilde{E})_\sigma \\ &\quad - (\partial_t \lambda, \tilde{E})_{\Gamma_T} + (\nabla \lambda, \nabla \tilde{E}) + (\nabla \cdot \lambda, \nabla \cdot (\varepsilon - 1)\tilde{E}), \end{aligned} \quad (21)$$

$$\begin{aligned} \frac{\partial L}{\partial \lambda}(u)(\tilde{\lambda}) &= -(\tilde{\lambda}(x, 0), f_1)_{\varepsilon, \Omega} - (\partial_t \tilde{\lambda}, \partial_t E)_\varepsilon + (\tilde{\lambda}, \partial_t E)_\sigma + (\tilde{\lambda}, \partial_t E)_{\Gamma_T} \\ &\quad + (\nabla \tilde{\lambda}, \nabla E) + (\nabla \cdot \tilde{\lambda}, \nabla \cdot (\varepsilon - 1)E), \end{aligned} \quad (22)$$

$$\frac{\partial L}{\partial \varepsilon}(u)(\tilde{\varepsilon}) = \gamma_\varepsilon(\varepsilon - \varepsilon^0, \tilde{\varepsilon})_\Omega - (\tilde{\varepsilon} \lambda(x, 0), f_1)_\Omega - (\tilde{\varepsilon} \partial_t \lambda, \partial_t E) + (\nabla \cdot \lambda, \nabla \cdot \tilde{\varepsilon} E), \quad (23)$$

$$\frac{\partial L}{\partial \sigma}(u)(\tilde{\sigma}) = \gamma_\sigma(\sigma - \sigma^0, \tilde{\sigma})_\Omega + (\tilde{\sigma} \lambda, \partial_t E). \quad (24)$$

By equating all these derivatives to 0 we have expressions for stationary points of L .

We observe that the derivative of the Lagrangian with respect to λ gives us the forward problem. Next, the derivative of the Lagrangian with respect to E gives us the adjoint problem, which reads

$$\varepsilon \partial_{tt} \lambda - \sigma \partial_t \lambda - (\varepsilon - 1) \nabla \nabla \cdot \lambda - \Delta \lambda = 0 \quad \text{in } \Omega_T, \quad (25)$$

$$\lambda(\cdot, T) = \partial_t \lambda(\cdot, T) = 0 \quad \text{in } \Omega, \quad (26)$$

$$\partial_n \lambda = \partial_t \lambda - (E - E_{\text{obs}})z \quad \text{on } \Gamma_T. \quad (27)$$

Note that for the adjoint problem we have swapped some signs of time derivatives, as well as given end time conditions, and this is also reflected in implementations where it is solved backwards in time.

Adjoint problem: Find λ which solves problem (25)–(27) for given functions ε , σ and E_{obs} .

5 Domain decomposition hybrid method

For practical implementation we of course need discrete schemes. We will present the semi-discrete schemes in this article to showcase how we use the domain decomposition and coefficient assumptions (13) for efficient solving of the forward problem. A lot of the details surrounding the actual numerical implementations are omitted (see [8] for more details), this section will mainly describe the communication between solutions on Ω_{FDM} and Ω_{FEM} .

First, let us define the partition on our finite element subdomain Ω_{FEM} ,

$$\overline{\Omega}_{\text{FEM}} := K_h := \cup_{K \in K_h} K, \quad (28)$$

where we assume that K_h obeys the minimum angle condition [26]. Using this partition K_h we define the finite element space for every component of the electric field:

$$V_h^E := \{w \in H^1(\Omega_T) : w|_K \in P^1(\Omega), \forall K \in K_h\}. \quad (29)$$

We can now state the finite element problem as finding $E_h \in V_h^E$ such that

$$\begin{aligned} & (\partial_{tt} E_h, v)_{\varepsilon, \Omega_{\text{FEM}}} + (\partial_t E_h, v)_{\sigma, \Omega_{\text{FEM}}} + (\nabla E_h, \nabla v)_{\Omega_{\text{FEM}}} - (\partial_n E_{\text{FD}}, v)_{\Omega_{\text{FEM}}} \\ & + (\nabla \cdot (\varepsilon - 1) E_h, \nabla \cdot v)_{\Omega_{\text{FEM}}} = 0, \end{aligned} \quad (30)$$

$$(E(x, 0), v(x, 0))_{\Omega_{\text{FEM}}} = (f_0, v(x, 0))_{\Omega_{\text{FEM}}}, \quad (31)$$

$$(\partial_t E(x, 0), v(x, 0))_{\Omega_{\text{FEM}}} = (f_1, v(x, 0))_{\Omega_{\text{FEM}}}, \quad (32)$$

for all $v \in V_h^E$ and $t \in (0, T)$. Here E_{FD} is the solution which is calculated using finite difference methods in Ω_{FDM} . Note that this altered boundary condition is essential to communicate between Ω_{FDM} and Ω_{FEM} , and we will have a similar condition for the finite difference method. We will not discuss the details in this article of solving (30)–(32) using finite element methods, but again point the reader to [8] for a more thorough description.

For the subdomain Ω_{FDM} where we implement finite difference methods, we instead solve the system below.

$$\partial_{tt} E_h - \Delta E_h = 0, \quad \text{in } \Omega_{\text{FDM}} \times (0, T) \quad (33)$$

$$E_h(x, 0) = f_{0h}(x), \quad \text{in } \Omega_{\text{FDM}}, \quad (34)$$

$$\partial_t E_h(x, 0) = f_{1h}(x), \quad \text{in } \Omega_{\text{FDM}}, \quad (35)$$

$$\partial_n E_h = -\partial_t E_h, \quad \text{in } \Gamma_T \quad (36)$$

$$\partial_n E_h = \partial_n E_{\text{FE}} \quad \text{in } (\partial\Omega_{\text{FDM}} \cap \Omega_{\text{FEM}}) \times (0, T) \quad (37)$$

Here E_{FE} is the solution attained on the subdomain Ω_{FEM} and f_{0h} and f_{1h} are nodal interpolations of f_0 and f_1 , correspondingly. Again, we omit the details of the actual finite difference implementation and refer to [8] for them.

Remark: We do not present it here, but the method is similarly applied for the adjoint problem as well.

6 Conjugate gradient method

To minimize the Lagrangian and thus reconstruct coefficients ε , σ , we aim to find it's stationary points as earlier mentioned. We also use the derivatives to inform the search direction for minimizers and apply a conjugate gradient method. We define the following functions to express said search direction pointwise:

$$\begin{aligned} g_\varepsilon(x) := & \gamma_\varepsilon(\varepsilon - \varepsilon^0)(x) - \lambda(x, 0) f_1(x) \\ & - \int_0^T (\partial_t \lambda(x), \partial_t E(x) - \nabla \cdot \lambda(x) \nabla \cdot E(x)) dt, \end{aligned} \quad (38)$$

$$g_\sigma(x) := \gamma_\sigma(\sigma - \sigma^0)(x) + \int_0^T \lambda(x) \partial_t E(x) dt. \quad (39)$$

Since the algorithm we will introduce is iterative, so we will represent this with a superscript, i.e. ε^m and σ^m are the coefficients reached on iteration m . Logically we will also denote $E^m := E(\varepsilon^m, \sigma^m)$, $\lambda^m := \lambda(E^m, \varepsilon^m, \sigma^m)$, $g_\varepsilon^m := g_\varepsilon^m(x)$ and $g_\sigma^m := g_\sigma^m(x)$ where $E(\varepsilon^m, \sigma^m)$ and $\lambda(E^m, \varepsilon^m, \sigma^m)$ are the solutions to the corresponding forward and adjoint problems, respectively. We can now state our conjugate gradient algorithm.

Conjugate Gradient Algorithm (CGA): For iterations $m = 0, \dots, M$ follow the steps below.

0. Let $m = 0$ and choose some initial guesses ε^0, σ^0 .

1. Calculate $E^m, \lambda^m, g_\varepsilon^m$ and g_σ^m .

2. Compute

$$\varepsilon^{m+1} := \varepsilon^m + \alpha_\varepsilon d_\varepsilon^m, \quad d_\varepsilon^m := -g_\varepsilon^m + \beta_\varepsilon^m d_\varepsilon^{m-1}, \quad \beta_\varepsilon^m := \frac{\|g_\varepsilon^m\|_\Omega^2}{\|g_\varepsilon^{m-1}\|_\Omega^2}, \quad (40)$$

$$\sigma^{m+1} := \sigma^m + \alpha_\sigma d_\sigma^m, \quad d_\sigma^m := -g_\sigma^m + \beta_\sigma^m d_\sigma^{m-1}, \quad \beta_\sigma^m := \frac{\|g_\sigma^m\|_\Omega^2}{\|g_\sigma^{m-1}\|_\Omega^2}, \quad (41)$$

where $\alpha_\varepsilon, \alpha_\sigma$ are chosen step size and with $d_\varepsilon^0 := -g_\varepsilon^0, d_\sigma^0 := -g_\sigma^0$.

3. Terminate the algorithm if either $\|\varepsilon^{m+1} - \varepsilon^m\| < \eta_\varepsilon^1$ or $\|\sigma^{m+1} - \sigma^m\| < \eta_\sigma^1$ and $\|g_\varepsilon^m\| < \eta_\varepsilon^2$ or $\|g_\sigma^m\| < \eta_\sigma^2$, where $\eta_\varepsilon^1, \eta_\varepsilon^2, \eta_\sigma^1$ and η_σ^2 are tolerances chosen by the user. Otherwise, set $m := m + 1$ and repeat the algorithm from step 1).

Remark: The algorithm was introduced in a continuous setting, but applies analogously in the discrete setting.

7 Adaptive Conjugate Gradient Algorithm

To keep computational times reasonable while still achieving desirable accuracy we therefore implement adaptive mesh refinement in regions of special interest. The criteria for these refinements depend on the magnitude of ε and σ . Mathematically this is motivated by the nature of the a posteriori errors between the discretized inverse problem solution ε_h and the optimizer for the Tikhonov functional ε_γ (see [9]), but from the perspective of our applications it makes sense as well, since tumours are correlated with higher values of ε .

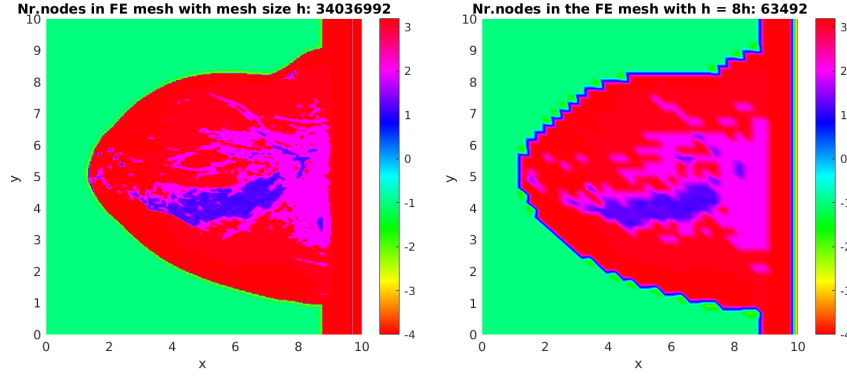


Figure 2: 2D presentation of media numbers for breast phantom with ID_012204 of database [28]. Left figure presents media numbers shown on the original mesh. Right figure shows media numbers on the sampled mesh where the mesh size was $8h$, h is the mesh size of the original mesh.

Adaptive Conjugate Gradient Algorithm (ACGA): For mesh refinements $i = 0, \dots$ follow the steps below.

0. Choose initial spatial mesh K_h^0 in Ω_{FEM} .
1. Calculate $\varepsilon_{h,i}$, $\sigma_{h,i}$ on mesh K_h^i according to the earlier introduced conjugate gradient method.
2. Refine elements in K_h^i such that

$$|h\varepsilon_{h,i}| + |h\sigma_{h,i}| \geq \beta \max_{K \in K_h^i} (|h\varepsilon_{h,i}| + |h\sigma_{h,i}|).$$

Here $h(x)|_K := \text{diam}(K)$ is the mesh function, and $\beta_t^\varepsilon, \beta_t^\sigma \in (0, 1)$ are constants chosen by the user.

3. Define the new mesh as K_h^{i+1} and interpolate $\varepsilon_{h,i}$, $\sigma_{h,i}$ as well as measurements E_{obs} onto it. Terminate the algorithm if either $\|\varepsilon_{h,i+1} - \varepsilon_{h,i}\| < \theta_\varepsilon^1$ or $\|\sigma_{h,i+1} - \sigma_{h,i}\| < \theta_\sigma^1$ and $\|g_\varepsilon^m\| < \theta_\varepsilon^2$ or $\|g_\sigma^m\| < \theta_\sigma^2$, where $\theta_\varepsilon^1, \theta_\varepsilon^2, \theta_\sigma^1$ and θ_σ^2 are tolerances chosen by the user. Otherwise, increase i by 1 and repeat the algorithm from step 1).

Remark: The mesh refinement algorithm was introduced in a semi-discrete setting, thus we have omitted the temporal mesh refinement. With a fully discrete scheme one also has to make sure that CFL conditions are met, since we are implementing explicit schemes (see details in [5], [8])

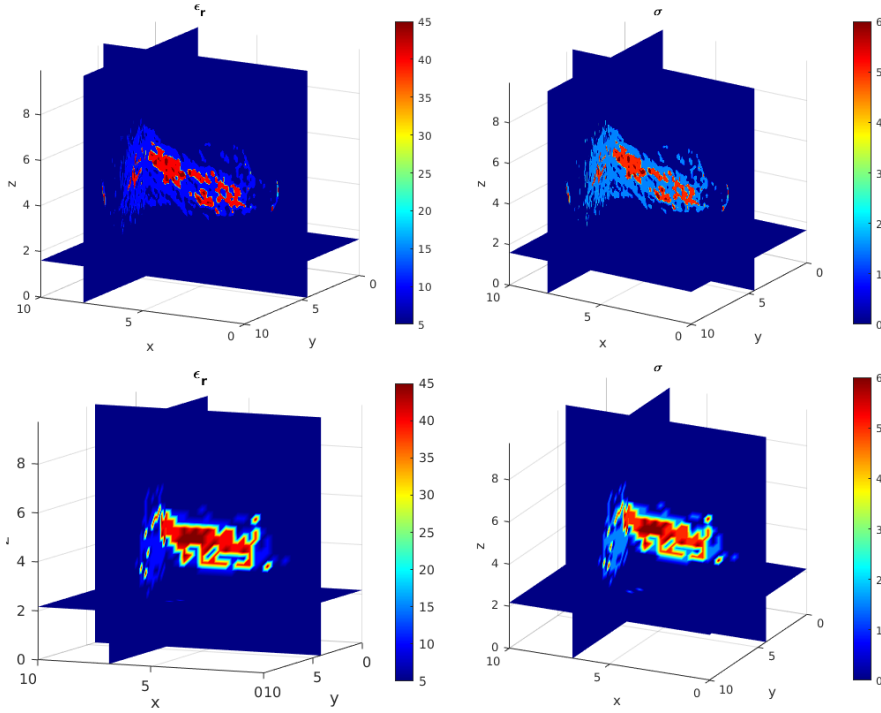


Figure 3: Dielectric properties at 6GHz of breast phantom with ID_012204 of [28] taken in our computations. Left images: ϵ_r , right images: σ . Top row presents original images on the mesh with number of nodes 34036992. Bottom row presents sampled values of ϵ_r and σ on the mesh with number of nodes 63492, where the mesh size was $8h$, h is the mesh size of the original mesh.

8 Numerical results

This section presents numerical results of the reconstruction of the relative dielectric permittivity function of the anatomically realistic breast phantom of object ID_012204 of online repository [28] using ACGA. In our numerical computations we use assumption that the effective conductivity function is known inside domain of interest. We refer to [8, 9] for details about numerical implementation and we use the same computational set-up as in [9].

Figure 2 presents distribution of media numbers for breast phantom with ID_012204 of database [28]. Figure 3 shows exact values of the relative dielectric permittivity and conductivity functions which we wanted to reconstructed in our numerical examples. Dielectric properties shown on this figure correspond to types of material presented on Figure 2, see also Table 1 for the description of tissue types used in our experiments.

Tissue type	media number	$\epsilon_r (\epsilon_r/5)$	$\sigma (\sigma/5)$
Immersion medium	-1	5 (1)	0 (0)
Skin	-2	5 (1)	0 (0)
Muscle	-4	5 (1)	0 (0)
Fibroconnective/glandular 1	1.1	45 (9)	6 (1.2)
Fibroconnective/glandular 2	1.2	40 (8)	5 (1)
Fibroconnective/glandular 3	1.3	40 (8)	5 (1)
Transitional	2	5 (1)	0 (0)
Fatty-1	3.1	5 (1)	0 (0)
Fatty-2	3.2	5 (1)	0 (0)
Fatty-3	3.3	5 (1)	0 (0)

Table 1: Tissue types and corresponding media numbers of database [28]. Dielectric properties as well as weighted dielectric properties for breast phantom with ID_012204 taken in our numerical computations are also presented. See Figure 2 for spatial distribution of media numbers and Figure 3 for spatial distribution of dielectric properties on original and sampled meshes.

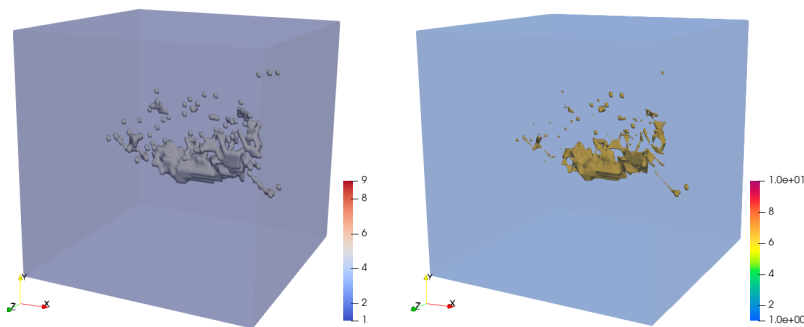


Figure 4: Left figure: exact isosurface of ϵ_r and right figure: finite element reconstruction ϵ_{r_h} (outlined in yellow color) corresponding to tissue types fibroconnective/glandular 2,3 obtained on two times refined finite element mesh K_{h_2} . The noise level in the data is $\delta = 10\%$.

Figure 4 presents reconstruction of weighted values of relative dielectric permittivity function obtained on two times adaptive locally refined meshes when we take an initial guess $\epsilon^0 = 6$ for tissue types Fibroconnective/glandular 1,2,3 and $\epsilon^0 = 1$ at all other points of the computational domain. Our computational tests show that an initial guess $\epsilon^0 \in [6, 8]$ for tissue types Fibroconnective/glandular 1,2,3 and $\epsilon^0 = 1$ at all other points of the computational domain provides good reconstructions of the maximum of the exact relative dielectric permittivity function.

9 Conclusions

The paper presents a hybrid finite element/finite difference method for reconstructions of dielectric properties of conductive object using adaptive conjugate gradient algorithm.

Our computational tests show qualitative and quantitative reconstruction of the relative dielectric permittivity function under the condition that the conductivity function

is known. All computational tests were performed using anatomically realistic breast phantom of MRI database produced in University of Wisconsin [28].

Future computational work is concerned with reconstruction of both dielectric permittivity as well as conductivity functions, in the time-dependent Maxwell equation, together with further testing on phantoms of online repository [28].

References

- [1] A. B. Bakushinsky, M. Yu. Kokurin, *Iterative Methods for Approximate Solution of Inverse Problems*, Springer, Dordrecht, The Netherlands, 2004.
- [2] L. Beilina, M. V. Klibanov, *Approximate global convergence and adaptivity for Coefficient Inverse Problems*, Springer, New York, 2012.
- [3] L. Beilina, M. Klibanov, *A posteriori error estimates for the adaptivity technique for the Tikhonov functional and global convergence for a coefficient inverse problem*, *Inverse Problems*, 26, 045012, 2010.
- [4] L. Beilina, V. Ruas, *On the Maxwell-wave equation coupling problem and its explicit finite element solution*, *Applications of Mathematics*, Springer, 2022. <https://doi.org/10.21136/AM.2022.0210-21>
- [5] L. Beilina, V. Ruas, *Explicit P_1 Finite Element Solution of the Maxwell-Wave Equation Coupling Problem with Absorbing b. c.*, *Mathematics*, 12(7), 936, 2024. <https://doi.org/10.3390/math12070936>
- [6] L. Beilina, N. T. Thành, M. Klibanov, M. A. Fiddy, *Reconstruction from blind experimental data for an inverse problem for a hyperbolic equation*, *Inverse Problems*, 30, 2014.
- [7] L. Beilina, N. T. Thành, M.V. Klibanov, J. B. Malmberg, *Globally convergent and adaptive finite element methods in imaging of buried objects from experimental backscattering radar measurements*, *Journal of Computational and Applied Mathematics*, Elsevier, 2015. DOI: 10.1016/j.cam.2014.11.055
- [8] L. Beilina, E. Lindström, *An Adaptive Finite Element/Finite Difference Domain Decomposition Method for Applications in Microwave Imaging*, *Electronics*, 11(9), 1359, 2022. <https://doi.org/10.3390/electronics11091359>
- [9] L. Beilina, E. Lindström, *A posteriori error estimates and adaptive error control for permittivity reconstruction in conductive media*, *Gas Dynamics with Applications in Industry and Life Sciences*, Springer Proceedings in Mathematics & Statistics, Springer, PROMS, vol.429, Cham, 2023.
- [10] M. de Buhan, M. Kray, *A new approach to solve the inverse scattering problem for waves: combining the TRAC and the adaptive inversion methods*, *Inverse Problems*, 29(8), 2013.

- [11] H. W. Engl, M. Hanke, A. Neubauer, *Regularization of Inverse Problems*, Kluwer Academic Publishers, Dordrecht, The Netherlands, 1996.
- [12] G. Chavent, *Nonlinear Least Squares for Inverse Problems. Theoretical Foundations and Step-by- Step Guide for Applications*, Springer, New York, 2009.
- [13] Gleichmann, Yannik G., Grote, Marcus J., *Adaptive Spectral Inversion for Inverse Medium Problems*, *Inverse Problems*, 39(12), 2023. DOI: 10.1088/1361-6420/ad01d4
- [14] A. V. Goncharsky, S. Y. Romanov, *A method of solving the coefficient inverse problems of wave tomography*, *Comput. Math. Appl.*, 77, 967–980, 2019.
- [15] A. V. Goncharsky, S. Y. Romanov, S. Y. Seryozhnikov, *Low-frequency ultrasonic tomography: mathematical methods and experimental results*, *Moscow University Phys Bullet*, 74(1), 43–51, 2019.
- [16] B. Jiang, *The Least-Squares Finite Element Method. Theory and Applications in Computational Fluid Dynamics and Electromagnetics*, Springer-Verlag, Heidelberg, 1998.
- [17] B. Jiang, J. Wu L. A. Povinelli, *The origin of spurious solutions in computational electromagnetics*, *Journal of Computational Physics*, 125, pp.104–123, 1996.
- [18] J. Jin, *The finite element method in electromagnetics*, Wiley, 1993.
- [19] Vo Anh Khoa, Grant W. Bidney, Michael V. Klibanov, Loc H. Nguyen, Lam H. Nguyen, Anders J. Sullivan, Vasily N. Astratov, *An inverse problem of a simultaneous reconstruction of the dielectric constant and conductivity from experimental backscattering data*, *Inverse Problems in Science and Engineering*, 29:5, 712-735, 2021. DOI: 10.1080/17415977.2020.1802447
- [20] N. T. Thánh, L. Beilina, M. V. Klibanov, M. A. Fiddy, *Reconstruction of the refractive index from experimental backscattering data using a globally convergent inverse method*, *SIAMJ. Sci. Comput.*, 36 (2014), pp. B273-B293.
- [21] N. T. Thánh, L. Beilina, M. V. Klibanov, M. A. Fiddy, *Imaging of Buried Objects from Experimental Backscattering Time-Dependent Measurements using a Globally Convergent Inverse Algorithm*, *SIAM Journal on Imaging Sciences*, 8(1), 757-786, 2015.
- [22] A. N. Tikhonov, A. V. Goncharsky, V. V. Stepanov, A. G. Yagola, *Numerical Methods for the Solution of Ill-Posed Problems*, London, Kluwer, 1995.
- [23] K. Ito, B. Jin, *Inverse Problems: Tikhonov theory and algorithms*, Series on Applied Mathematics, V.22, World Scientific, 2015.
- [24] W.T. Joines, Y. Zhang, C. Li, R. L. Jirtle, *The measured electrical properties of normal and malignant human tissues from 50 to 900 MHz*, *Med. Phys.*, 21 (4), pp.547-550, 1994.

- [25] S. Kabanikhin, A. Satybaev, M. Shishlenin, *Direct Methods of Solving Multidimensional Inverse Hyperbolic Problems*, VSP, Utrecht, The Netherlands, 2004.
- [26] M. Křížek, P. Neittaanmäki, *Finite element approximation of variational problems and applications*, Longman, Harlow, 1990.
- [27] P.B. Monk, *Finite Element Methods for Maxwell's Equations*, Oxford University Press: Oxford, UK, 2003.
- [28] E. Zastrow, S. K. Davis, M. Lazebnik, F. Kelcz, B. D. Veen, S. C. Hagness, *Online repository of 3D Grid Based Numerical Phantoms for use in Computational Electromagnetics Simulations*, <https://uwcem.ece.wisc.edu/MRIdatabase/>